# Simultaneous Nonlinear Self-Interference Cancellation and Signal of Interest Recovery Using Dual Input Deep Neural Network in New Radio Access Networks

Qi Zhou<sup>®</sup>, Shuyi Shen<sup>®</sup>, You-Wei Chen<sup>®</sup>, Rui Zhang<sup>®</sup>, Jeff Finkelstein, and Gee-Kung Chang<sup>®</sup>, Fellow, IEEE

Abstract—An efficient method for simultaneous nonlinear selfinterference (SI) cancellation and signal-of-interest (SOI) recovery is proposed and experimentally verified in a mmWave over fiber testbed, based on a specially designed dual-input deep neural network (DI-DNN). The mmWave band has been adopted in the U.S. to provide 5G wireless access services due to its wide-bandwidth, lightof-sight propagation, and inherent compatibility with small cell architecture. To further meet the uprising bandwidth-demanding services, the in-band full-duplex (IBFD) scheme is introduced to magnify the mmWave channel capacity for the 5G and beyond wireless communications. Fortunately, the mmWave band is more realistic to implement IBFD compared with the conventional sub-6GHz band, as it operates as a highly directional beam and shorter transmission distance resulting in a higher SOI to SI ratio. In our proposed solution, a DI-DNN is, for the first time, proposed and implemented to simultaneously realize the SI cancellation and the SOI recovery. Moreover, we firstly mitigate the nonlinearity arising from the transmitters of both the SI and SOI, as well as the nonlinear crosstalk from the SI to the SOI after detection by a nonlinear receiver. The demonstration of the DI-DNN joint with the experimental implementation in a mmWave over fiber system, promise spectral efficient, high-capacity signal transport in the 5G and beyond wireless communications.

Index Terms—Deep neural network, mmWave over fiber, self-interference cancellation.

# I. INTRODUCTION

HE 5G radio access network (RAN) has been undergone dramatic innovations recently by adopting the mmWave band to enhance the channel usable spectrum and capacity [1]. Besides, flexible function split among centralized unit (CU),

Manuscript received September 11, 2020; revised December 8, 2020; accepted December 14, 2020. Date of publication December 16, 2020; date of current version April 2, 2021. This work was supported by a Research Grant from Cox Communications under Grant 102059. (Corresponding author: Qi Zhou.)

Qi Zhou, Shuyi Shen, You-Wei Chen, Rui Zhang, and Gee-Kung Chang are with the School of Electrical and Computer Engineering, Georgia Institute of Technology, Atlanta, GA 30308 USA (e-mail: qi.zhou@gatech.edu; ssyzoe@gatech.edu; yu-wei.chen@ece.gatech.edu; ruizhangece@gatech.edu; gkchang@ece.gatech.edu).

Jeff Finkelstein is with Cox Communications, Atlanta, GA 30328 USA (e-mail: jeff.finkelstein@cox.com).

Color versions of one or more figures in this article are available at https://doi.org/10.1109/JLT.2020.3045368.

Digital Object Identifier 10.1109/JLT.2020.3045368

distributed unit (DU), and remote radio unit (RRU) are introduced to enable dynamic and scalable configuration of RAN to support diverse use cases including enhanced mobile broadband (eMBB), ultra-reliable ultra-low-latency (uRLLC) services, etc [2]–[3]. The CU, DU, and RRU are fiber connected to satisfy the huge bandwidth requirements. Meanwhile, unlike conventional time-division duplex (TDD) and frequency-division duplex (FDD), in-band full-duplex (IBFD) communication has drawn tremendous interest as it uses the same physical resource for bi-directional transmission and could be used as a standalone technique or complementing mmWave to increase channel capacity [4]. Inevitably, severe self-interference (SI) from downlink signal would overwhelm the signal-of-interest (SOI), i.e., uplink signal, at the base station receiver due to the approximation of the collocated transmit antenna and receive antenna. Enabling the IBFD relies on efficient cancellation schemes to suppress the Tx SI. The SI cancellation scheme is mainly categorized into passive suppression, analog cancellation, and digital cancellation. In passive suppression, the SI signal is suppressed at the Tx-Rx air interface using antenna configuration and design to lessen coupling between Tx and Rx [5]. In active cancellation, the SI signal is cancelled via subtracting a reconstructed SI copy from the known Tx signal. The active cancellation can be further divided into analog and digital cancellation, based on the processing domain (analog or digital) of where the SI is subtracted. Various analog interference cancellers based on electronics or optics have been reported in [6]-[9]. In [8], we demonstrated a 30-dB cancellation depth over 5.5-GHz bandwidth based on an optoelectronics canceller. However, the analog canceller is typically costly and not efficient or scalable to remove the SI after a non-ideal channel response. In this case, digital cancellation can be implemented to cancel the remaining SI components after the dominant SI is mitigated by an analog canceller. The basic idea of the conventional digital SI cancellation is to estimate the channel coefficients between the local transmitter and the receiver. Based on the estimated coefficients, a SI cancellation signal is constructed to subtract the SI from the received signal [10]–[11]. However, those reported digital cancellation schemes lack the analysis and consideration of SI cancellation and SOI recovery when the channels exhibit nonlinearities. In those cases, the remaining nonlinear SI after

0733-8724 © 2020 IEEE. Personal use is permitted, but republication/redistribution requires IEEE permission. See https://www.ieee.org/publications/rights/index.html for more information.

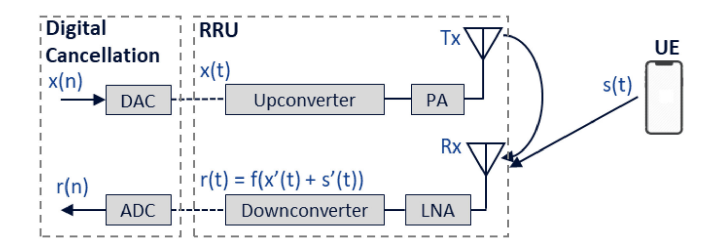


Fig. 1. Simplified full-duplex wireless communication diagram. PA: power amplifier; LNA: low-noise amplifier; RRU: remote radio unit; UE: user equipment.

conventional analog and digital cancellation is still inevitable and degrades the SOI quality significantly. To address those challenges, ordinary neural networks are introduced to construct a non-linear SI cancellation signal [12]–[14], which has less computation complexity at the inference step (i.e., after training is completed) than nonlinear polynomial-based methods (Volterra series). However, those results assume the receiver operating linearly such that the SI can be removed by simple subtraction. On the other hand, any receiver nonlinearity would cause inaccurate SI channel estimation such that the subtraction-based digital cancellation schemes would fail to suffice.

In this paper, we propose a DI-DNN based interference canceller for simultaneous SI cancellation and SOI recovery, taking both the received signal and the known SI as dual inputs to the neural networks. We conduct a proof-of-concept experiment based on an mmWave over fiber platform to verify the performance of the proposed interference canceller systematically. To the best of our knowledge, this is the first attempt for simultaneous SI cancellation and SOI recovery considering receiver nonlinearity, along with pilot feasibility evaluation on mmWave band full duplex.

# II. OPERATING PRINCIPLES

This section review and explain the fundamentals of polynomial interference canceller and the principles of neural networks based cancellers. Fig. 1 shows a simplified wireless full-duplex system diagram to help explain different cancellers' models and principles. The digital baseband signal at time instant n is denoted as x(n). The signal is converted by a digital-to-analog converter (DAC) into the analog domain, then is upconverted and amplified before being transmitted by the base station (BS) antenna. Here, we denote the signal's baseband equivalent as x(t). Due to the proximity of the transmit and receive antenna, the transmitted x(t) causes severe SI at the local receiver. At the user equipment (UE) side, s(t) is generated and sent to the BS as the SOI. At the BS receiver, after amplification and downconversion, r(t) is obtained with received SOI s'(t) superimposed with the strong received SI x'(t). The r(n) represented the digital baseband of r(t) = f(x'(t) + s'(t)) after the analog-to-digital converter (ADC), where f represents a nonlinear transfer function at the BS receiver. Besides, the digital SI cancellation and DSP part do not need to be located at the BS based on different fronthaul function splits.

# A. Polynomial Interference Cancellers

To recover the SOI s(t) from the interfered received signal r(t), the received SI x'(t) needs to be cancelled. Assume  $h_{\rm SI}$  represents the impulse response of the SI channel, the received digital SI signal x'(n) can be modeled as

$$x'(n) = \sum_{l=-L}^{L} h_{SI}(l) x (n-l)$$
 (1)

where the memory length of the channel is 2L + 1. In polynomial interference cancellers, a SI cancellation signal  $\hat{x}(n)$  is constructed based on polynomial estimated  $h_{\rm SI}$  and can be derived by the Volterra series of x(n) as follows:

$$\hat{x}(n) = h_0 + \sum_{k=1}^{K} \sum_{l_1 = -L_1}^{L_1} \dots \sum_{l_K = -L_K}^{L_K} h_k(l_1, \dots, l_K)$$

$$\times \prod_{j=1}^{k} x(n - l_j)$$
(2)

Here, K is the highest nonlinearity order,  $L_k$  is the one-sided memory length, while  $2L_k+1$  represents the total memory length of the k-th order nonlinearity, and  $h_k$  is the coefficient for each Volterra series element. Based on the (2), the  $\hat{x}(n)$  can be estimated using the MMSE optimizer. In this case, the recovered SOI  $\hat{s}(n)=r(n)-\hat{x}(n)$ . The polynomial canceller assumes no nonlinear crosstalk between the SI and SOI, such that the SI can be directly subtracted from the received signal.

The polynomial canceller is normally associated with high computation complexity, especially when K is large (eg. K = 5). This computation complexity comes from a massive number of basis functions and the calculations of basis functions. As the multiplications dominate the hardware resources consumption, we evaluate the cancellers' complexity based on how many multiplications are required at the inference step. The complexity of the polynomial cancellers is:

$$N_{poly} = \sum_{k=1}^{K} C_k^{2L_k+k} + \sum_{k=1}^{K} (k-1) C_k^{2L_k+k} = \sum_{k=1}^{K} k C_k^{2L_k+k}$$
(3)

Here, the first item calculates the total number of the basis of a polynomial canceller, while the second item is the multiplications required for the basis function calculation. The linear canceller is a special case of the polynomial cancellers with K=1.

# B. Neural Networks Based Cancellers

The neural networks have demonstrated superior performance over the Volterra series in nonlinear equalizations [15], [16], such that an intuitive idea to use neural networks for interference cancellation is to estimate the  $h_{\rm SI}$  replacing the polynomial formula. Fig. 2 demonstrates a conventional DNN-based canceller structure. To make it simpler, we use  $I_{\rm N}\text{-}H_1\text{-}H_2\text{-}H_3\text{-}O_{\rm N}$  to represent the structure of the shown DNN. The processing flow is similar to polynomial cancellers but using a DNN for SI channel estimation. The total memory length for DNN input is

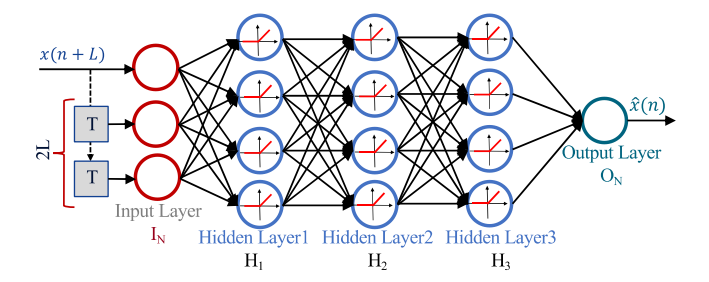


Fig. 2. Structure and parameters of a conventional DNN canceller.

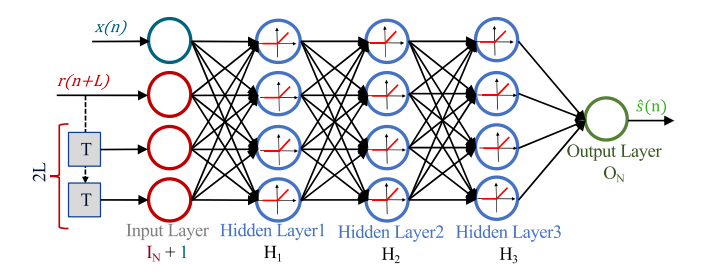


Fig. 3. Structure and parameters of the proposed DI-DNN canceller.

2L+1. In this case, the  $\hat{x}(n)=f_{DNN}(\sum_{l=-L}^L x(n-l))$ . The DNN canceller has a lower computation complexity than the compared polynomial cancellers based on pruned Volterra series at the inference step due to its narrow and deep architecture. The total complexity based on multiplications is:

$$N_{DNN} = I_N \times H_1 + H_D \times O_N + \sum_{i=1}^{i=D-1} H_i \times H_{i+1}$$
 (4)

Here,  $I_{\rm N}$  is the number of neurons at the DNN input layer,  $H_{\rm i}$  is the neurons' number at each hidden layer,  $O_{\rm N}$  is the output neuron number, and D is the depth of the DNN (the total number of the hidden layers).

Unfortunately, the intuitive DNN canceller is still subtraction-based, which cannot mitigate the nonlinear crosstalk from the SI to the SOI. In order to solve this limitation, we design a novel DI-DNN canceller. As shown in Fig. 3, the DI-DNN has two separate inputs, one is from the known current SI x(n) and the other input is the received signal r(n) with its L precursor and L postcursor samples. In this case, the SOI can be directly recovered as:

$$\hat{s}(n) = f_{DI-DNN}\left(x(n), \sum_{l=-L}^{l=L} r(n-l)\right)$$
 (5)

On account of the nonlinear Relu activation function at each hidden layer, the DI-DNN can capture and mitigate the nonlinear SI to SOI crosstalk, which significantly improves the SOI recovery performance. The DI-DNN only has a negligible complexity increase than DNN canceller due to the extra x(n) as the input:

$$N_{DI-DNN} = (I_N + 1) \times H_1 + H_D \times O_N$$

$$+ \sum_{i=1}^{i=D-1} H_i \times H_{i+1}$$

$$= N_{DNN} + H_1$$
(6)

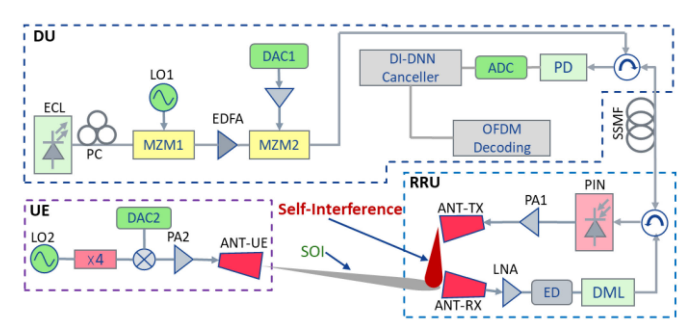


Fig. 4. Experimental setup of full-duplex mmWave over fiber access system.

The weights of the DI-DNN are optimized via supervised learning using training samples containing known inputs and corresponding outputs. The loss function is defined as the MSE and the loss with respect to the weights can be computed using backpropagation. The weight optimization is based on the Adam gradient descent algorithm, which implements momentum and adaptive learning rate during each weight update [17]. The gradient update rule at step t is:

$$m_{t} = \beta_{1} m_{t-1} + (1 - \beta_{1}) g_{t}$$

$$v_{t} = \beta_{2} v_{t-1} + (1 - \beta_{2}) g_{t}^{2}$$

$$w_{t} = w_{t-1} - \eta \frac{m_{t}}{\sqrt{v_{t}} + \epsilon}$$
(7)

The  $m_t$  is the exponential average gradients, the  $v_t$  is the exponential average of gradient squares, the  $g_t$  is the current gradient,  $\eta$  is the initial learning rate;  $\beta_1,~\beta_2$ , and  $\in$  are hyperparameters to fine-tune the Adam optimizer. This optimizer promises a fast and optimized convergence.

### III. EXPERIMENTAL SETUP

Based on a similar centralized digital interference cancellation and signal processing architecture as we proposed in [18], we conduct a proof-of-concept experiment to verify the feasibility of the DI-DNN interference canceller and compare its performance over the state-of-the-art subtraction based digital interference cancellation schemes, including linear, nonlinear, and the DNN.

Fig. 4 depicts the experimental setup and processing architecture. In the DU side, a C-band external cavity laser (ECL, PPCL100) is employed to generate an optical carrier to the Mach-Zehnder Modulator 1 (MZM1) biased at the null point. At the same time, a 30-GHz RF single-tone signal is modulating onto the MZM1 to obtain 60-GHz spacing optical sidebands based on optical carrier suppression (OCS). To compensate for the modulation loss from the MZM1, an EDFA (AEDFA13-B-FC) is used to boost the output optical signal. On the other hand, we generate a 16-QAM OFDM signal serving as the SI. The subcarrier spacing is  $2^7 \times 15 \text{ kHz} = 1.92 \text{ MHz}$  compliant with 5G conventions. The SI signal has 104 active carriers which imply a signal bandwidth of around 200 MHz, while the intermediate frequency is 300 MHz. The SI signal is digital-to-analog converted through a 16 GSa/s arbitrary waveform generator (AWG, M8195A) and boosted by a modulator driver (Picosecond 5865) to modulate the optical signal at the MZM2, which is biased at the quadrature point. The RRU is connected to the DU with a 15-km standard single-mode fiber (SSMF). After the detection by a V-band photodetector (XPDV2020R), an upconverted SI signal is generated with a 60-GHz carrier frequency. The SI signal is amplified by a 25-dB gain power amplifier (PA1) before entering a 15-dBi horn antenna. The transmit antenna is intentionally partially positioned toward the receive antenna to mimic strong self-interference. In the UE side, a random bit-sequence is generated and modulated into QPSK symbols, following by conventional OFDM DSP to serve as the SOI. The SOI has 52 active subcarriers with 1.92 MHz subcarrier spacing. The intermediate frequency is the same as the SI signal to intensify the in-band self-interference. The SOI is upconverted to 60-GHz carrier frequency via mixing with a quadrupled 15-GHz RF single tone signal. The UE antenna is placed 2-meters away from the RRU receive antenna and the power of the SOI is controlled to verify the digital cancellers performance under different SOI to SI power ratio. At the RRU receive antenna, both the SOI and SI are captured and amplified by a low-noise amplifier (LNA). The received signal is down-converted by an envelope detector (ED, DET-15-RPFW0). Since the RRU lacks processing capability, the received signal is sent back to the DU for the interference cancellation and DSP using a directly modulated laser (DML) based IM-DD link. A real-time oscilloscope (DSOZ254A) is used at the DU to sample the received signal to obtain data for experimental verification.

### IV. EXPERIMENTAL RESULTS AND ANALYSIS

Our experimental results mainly categorized into three parts: i) Convergence analysis and overfitting evaluation on the DI-DNN; ii) Detailed SI cancellation and SOI recovery demonstration at -6-dB SOI to SI power ratio; iii) Direct performance and complexity comparison among linear, nonlinear, DNN and DI-DNN cancellers at different SOI to SI power ratio.

# A. Convergence Analysis and Over-Fitting Evaluation

The proposed DI-DNN is implemented using the Tensorflow Keras framework. The DI-DNN consists of 1 input layer, 1 output layer and 3 hidden layers. The structure is (21 + 1)-8-4-4-1. We construct a feature dataset for the DI-DNN training and testing using the received signal samples and synchronized known SI samples with a dimension of 195820 by 22. Each feature dataset element consists of two separate inputs. The first input is formed by the currently received signal sample with its 10 precursor and 10 postcursor samples, while the second input is obtained from the current SI sample. The target dataset for the DI-DNN is built from the synchronized SOI samples with each element be the current SOI sample. The dimension of the target dataset is 195820 by 1. The first 2/3 of the dataset is used for DI-DNN training while the remaining 1/3 is used for testing. The initial step size of the Adam optimizer is set to 0.02, the mini-batch size is 8000, and the total training epoch is 100. Fig. 5 demonstrates the monitored training loss and testing loss over 100 epochs when the SOI to SI power ratio is -6 dB. The training loss and testing loss come very close to each other over the whole training epochs, the testing loss is even slightly smaller than the training loss because the training loss

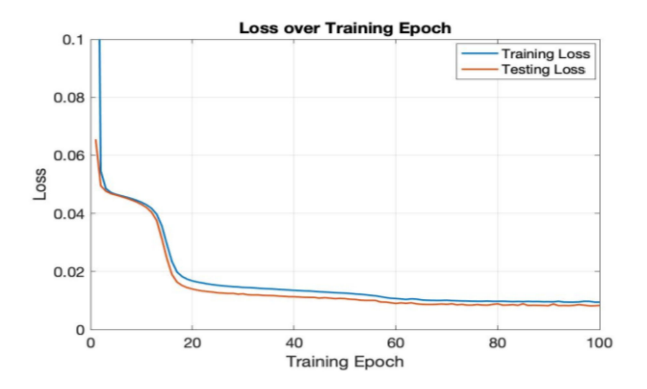


Fig. 5. Training and testing MSE loss over 100 training epochs.

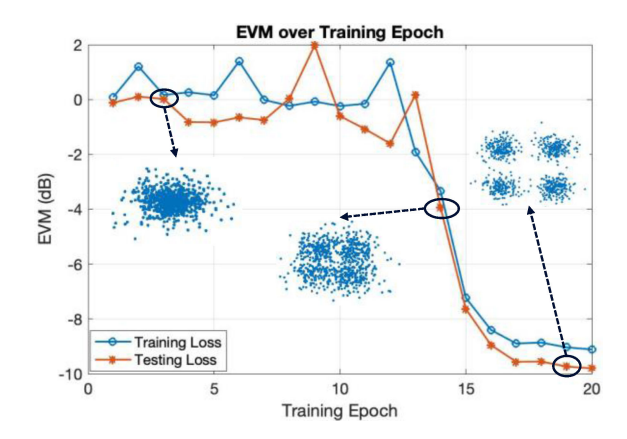


Fig. 6. EVM in dB and constellation of recovered SOI over the first 20 training epochs for both training and test set.

is measured during each epoch while testing loss is measured after each epoch. The close match of the training and testing loss verifies there is no overfitting. To connect the testing loss to SOI recovery performance, we plot the recovered SOI EVM in dB over the first 20 epochs, as the DI-DNN model already converges to a relatively low MSE loss (below 0.014) after epoch 20. As shown in Fig. 6, the recovered SOI EVM follows the trend of the descent training/testing loss. The insets show how the SOI recovers from a corrupted constellation (at epoch 3) to a clear constellation (at epoch 19) along with the model's evolution.

## B. SI Cancellation and SOI Recovery

At the last training epoch (epoch 100), the MSE loss converges to 0.008, such that the DI-DNN model is well-trained for performance evaluation. Fig. 7 demonstrates the constellation and spectrum recovery of the SOI from the received signal. After applying the DI-DNN canceller, the EVM in dB of the SOI is improved from -0.2 dB to -;15.0 dB with a 14.8-dB gain achieved. The recovered constellation is clear and the SOI spectrum is fully recovered from a completely overwhelmed received spectrum. To visualize the subtraction of SI and the recovery of SOI in conventional cancellers, the received signal and the recovered signals are illustrated in the frequency domain. The hyper-parameter setting of the DNN canceller is similar to the DI-DNN for a fair comparison. Fig. 8 shows the spectrum of the received signal, linear, nonlinear, and DNN recovered

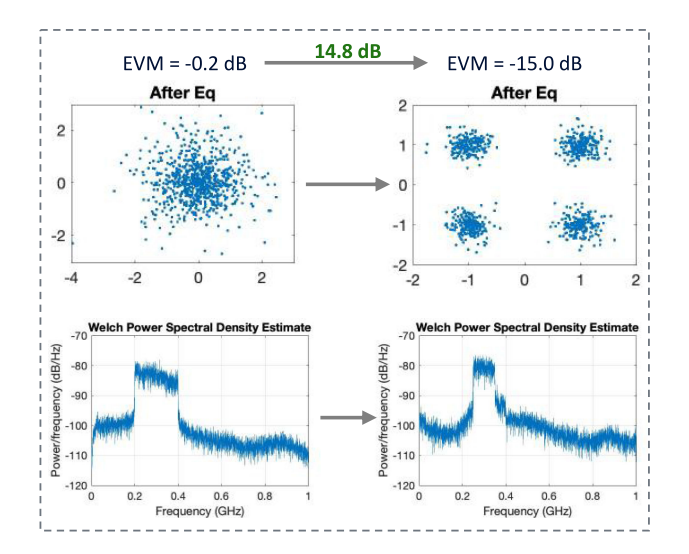


Fig. 7. Constellation and spectrum recovery of SOI based on the DI-DNN canceller.

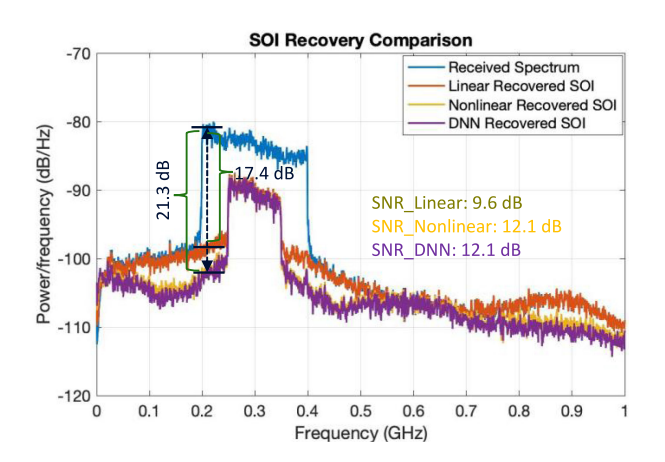


Fig. 8. Spectrum comparison between before and after cancellation of linear canceller, nonlinear canceller and DNN canceller.

SOI, respectively. Unlike many previous papers that evaluate the cancellation performance with only the presence of SI, we measure the metrics more realistically having the SI and SOI coexist in the received signal. As shown, the linear canceller has a 17.4-dB cancellation depth, resulting in a 9.6-dB SNR of the recovered SOI. The nonlinear canceller and the DNN canceller perform similarly, both show 21.3-dB cancellation and 12.1 dB recovered SNR. The extra 3.9-dB cancellation comes from a better estimation of the SI cancellation signal considering the transmitter side nonlinearity.

# C. Performance and Complexity Comparison

The SOI to SI power ratio is an important factor to evaluate the cancellers' performance, as its value significantly affects the nonlinear crosstalk from the SI to the SOI. Besides, with a higher SOI to SI ratio, the nonlinear channel estimation on SI will be less accurate, which remarkably degrades the conventional subtraction-based cancellers performance. Due to nonlinearity at the receiver, the received SI and SOI will compete for the received power. For example, –6-dB input SOI to SI ratio

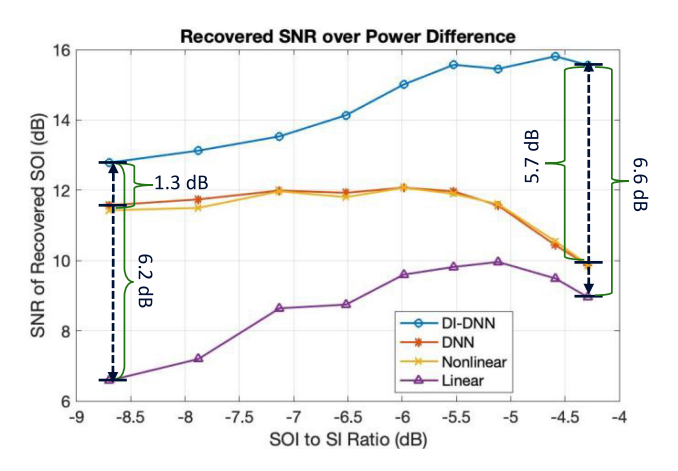


Fig. 9. SNR of recovered SOI comparison among linear, nonlinear, DNN and DI-DNN cancellers over input SOI to SI ratio.

corresponds to -9.3-dB received SOI to SI ratio. In the whole context, we refer the SOI to SI ratio as input SOI to SI ratio. Fig. 9 demonstrates the direct comparison of SOI recovery performance under different SOI to SI ratio. From the shown curves, the SNR of DI-DNN recovered SOI has 1.3-dB gain over the DNN and the nonlinear cancellers at -8.7-dB SOI to SI ratio. The gain is relatively small because the SI is dominant in the received signal, such that the nonlinear channel estimation on the SI is more accurate. Conversely, at -4.2-dB SOI to SI ratio, the DI-DNN canceller outperforms the DNN and the nonlinear cancellers by 5.7 dB. The huge margin results from a more accurate estimation of the SI cancellation signal, which is affected by the presence of the SOI, especially when the SOI is close to the SI in terms of power. This conclusion can also be justified by the declining trend of the red and yellow curve when SOI to SI ratio surpasses -6 dB, which indicates stronger nonlinear crosstalk between SOI and SI. The linear canceller performs poorly as shown by the purple curve. The DI-DNN demonstrates more than 6-dB gain over the whole SOI to SI ratio range.

Time complexity is another essential metric to evaluate potential real-time performance. Since the multiplication operations consume most of the hardware resources, here we take the total number of multiplications as the time complexity. Due to a similar neural network structure, the DI-DNN and the DNN cancellers' complexities are close to each other. Based on formula (4) and (6), the total multiplications required at the inference step are  $(21 + 1) \times 8 + 8 \times 4 + 4 \times 4 + 4 \times 1 = 228$ and  $21 \times 8 + 8 \times 4 + 4 \times 4 + 4 \times 1 = 220$ , respectively. The Volterra nonlinear canceller, on the other hand, has a much higher complexity. Its highest nonlinear order is 3, the linear memory length is 21, both the second and the third order nonlinear memory lengths are 11. Based on formula (3), the total multiplications required is  $21 + 66 + 286 + 66 + 286 \times 2 = 1011$ . The DI-DNN saves 77.5% required multiplications compared with the Volterra nonlinear canceller. However, if compared with simpler polynomial models like parallel Hammerstein, the complexity reduction would be smaller. Obviously, the linear canceller has the least complexity with only 21 multiplications

TABLE I COMPLEXITY COMPARISON

Methods	Computational Complexity (Multiplications Required)
DI-DNN	228
Conventional DNN	220
Volterra Canceller	1011
Linear Canceller	21

but at the cost of insufficient performance. The complexity comparisons are summarized in Table I.

### V. CONCLUSION

In this paper, for the first time, we propose a novel DI-DNN canceller for simultaneous nonlinear SI cancellation and the SOI recovery. We also conduct a proof-of-concept experiment based on the mmWave over fiber testbed to verify the DI-DNN performance and compare it with the conventional subtractionbased cancellers in terms of recovered SNR and complexity. The DI-DNN model exhibits negligible overfitting issue during the whole training epochs. After applying the trained DI-DNN, the EVM of the received SOI improves from the corrupted -0.2 dBto -15.0 dB with a clear recovered constellation. The DI-DNN canceller demonstrates significant SNR gain over the nonlinear and the DNN cancellers especially when the SOI to SI ratio is small. A remarkable 5.7-dB gain is realized at a ratio equals -4.3 dB. After the training is completed, the inference of the DI-DNN canceller saves 77.5% multiplications than Volterra nonlinear canceller. Therefore, the proposed DI-DNN canceller, together with the mmWave over fiber radio access system implementation serves as a promising candidate for the 5G and beyond full-duplex wireless communication networks.

# REFERENCES

- E. Dahlman, G. Mildh, S. Parkvall, J. Peisa, J. Sachs, and Y. Selén, "5G radio access," *Ericsson Rev.*, vol. 6, no. 1, pp. 2–6, 2014.
- [2] C.-Y. Chang, N. Nikaein, R. Knopp, T. Spyropoulos, and S. S. Kumar, "FlexCRAN: A flexible functional split framework over ethernet fronthaul in Cloud-RAN," in *Proc. IEEE Int. Conf. Commun. (ICC)*, 2017, pp. 1–7.

- [3] Y. Alfadhli, M. Xu, S. Liu, F. Lu, P.-C. Peng, and G.-K. Chang, "Real-time demonstration of adaptive functional split in 5G flexible mobile fronthaul networks," in *Proc. Opt. Fiber Commun. Conf.*, 2018, Paper Th2A–48.
- [4] S. Hong et al., "Applications of self-interference cancellation in 5G and beyond," *IEEE Commun. Mag.*, vol. 52, no. 2, pp. 114–121, Feb. 2014.
- [5] E. Everett, A. Sahai, and A. Sabharwal, "Passive self-interference suppression for full-duplex infrastructure nodes," *IEEE Trans. Wirel. Commun.*, vol. 13, no. 2, pp. 680–694, Feb. 2014.
- [6] J.-I. Choi, M. Jain, J. Shalizi, and J. Mehlman, "Systems and methods for frequency independent analog self-interference cancellation," U.S. Patent No. 9,036,749. May 19, 2015.
- [7] M. P. Chang, M. Fok, A. Hofmaier, and P. R. Prucnal, "Optical analog self-interference cancellation using electro-absorption modulators," *IEEE Microw. Wirel. Compon. Lett.*, vol. 23, no. 2, pp. 99–101, Feb. 2013.
- [8] Q. Zhou, H. Feng, G. Scott, and M. P. Fok, "Wideband co-site interference cancellation based on hybrid electrical and optical techniques," *Opt. Lett.*, vol. 39, no. 22, pp. 6537–6540, 2014.
- [9] Q. Zhou, J. Ge, and M. P. Fok, "Fast dynamic in-band RF self-interference cancellation for enabling efficient spectral usage," in *Proc. Opt. Fiber Commun. Conf.*, 2017, Paper W4B–5.
- [10] D. Korpi, L. Anttila, V. Syrjälä, and M. Valkama, "Widely linear digital self-interference cancellation in direct-conversion full-duplex transceiver," *IEEE J. Sel. Areas Commun.*, vol. 32, no. 9, pp. 1674–1687, Sep. 2014.
- [11] Z. Li, Y. Xia, W. Pei, K. Wang, and D. P. Mandic, "An augmented nonlinear LMS for digital self-interference cancellation in full-duplex direct-conversion transceivers," *IEEE Trans. Signal Process.*, vol. 66, no. 15, pp. 4065–4078, Aug. 2018.
- [12] A. Balatsoukas-Stimming, "Non-linear digital self-interference cancellation for in-band full-duplex radios using neural networks," in *Proc. IEEE 19th Int. Workshop Signal Process. Adv. Wireless Commun. (SPAWC)*, 2018, pp. 1–5.
- [13] A. T. Kristensen, A. Burg, and A. Balatsoukas-Stimming, "Advanced machine learning techniques for self-interference cancellation in full-duplex radios," in *Proc. 53rd Asilomar Conf. Signals, Syst., Comput.*, 2019, pp. 1149–1153.
- [14] C. Shi, Y. Hao, Y. Liu, and S. Shao, "Digital self-interference cancellation for full duplex wireless communication based on neural networks," in *Proc.* 4th Int. Conf. Commun. Inf. Syst. (ICCIS), 2019, pp. 53–57.
- [15] Q. Zhou et al., "Enhanced multi-level signal recovery in mobile fronthaul network using DNN decoder," *IEEE Photon. Technol. Lett.*, vol. 30, no. 17, pp. 1511–1514, Sep. 2018.
- [16] S. Liu, Y. M. Alfadhli, S. Shen, M. Xu, H. Tian, and G.-K. Chang, "A novel ANN equalizer to mitigate nonlinear interference in analog-RoF mobile fronthaul," *IEEE Photon. Technol. Lett.*, vol. 30, no. 19, pp. 1675–1678, Oct. 2018.
- [17] D. P. Kingma and J. Ba, Adam: A method for stochastic optimization, 2014. [Online] Available: https://arxiv.org/abs/1412.6980
- [18] Q. Zhou et al., "Centralized digital self-interference cancellation technique to enable Full-duplex operation of next generation millimeter wave over fiber systems," in *Proc. Opt. Fiber Commun. Conf. Exhib. (OFC)*, 2020, pp. 1–3.